ECS Transactions, 68 (1) 2129-2139 (2015)
10.1149/06801.2129ecst ©The Electrochemical Society

Fabrication and Microstructure of Self-Supporting Thin Ceramic Electrolytes Prepared by Laser Machining

J. A. Cebollero, R. Lahoz, M. A. Laguna-Bercero, J. I. Peña, A. Larrea and V.M. Orera

Instituto de Ciencia de Materiales de Aragón, U. Zaragoza-CSIC
C/ María de Luna 3, E-50.018 Zaragoza, Spain

Self-supporting thin Yttria Stabilized Zirconia (YSZ) ceramic electrolytes have been prepared by laser machining. They are carved from a sintered YSZ plate to shape a 20 μm thick and 8 mm in diameter central region, surrounded by an unprocessed 150 μm thick supporting zone. Scanning Electron Microscopy (SEM) and Electron Back Scattering Diffraction (EBSD) studies confirmed that the strains produced by the laser processing are small and limited to only one or two layers of YSZ grains (~5 μm). SEM and Transmission Electron Microscopy (TEM) have been also used to characterize the surface of the membrane. It is corrugated and coated with YSZ nanoparticles as a result of the laser plasma deposition. Electrochemical characterization by Impedance Spectroscopy (EIS) showed that this surface morphology improves the electrical performance of the membrane slightly but clearly, reducing the cathode polarization resistance by about 5% in the 650-850 ºC range.

Introduction

The Solid Oxide Fuel Cells (SOFC) are electrochemical devices that transform the energy stored in chemical compounds (fuel) into work (electricity) and heat (hot water). They carry out this transformation cleanly, silently and with high efficiency (1). One of the most relevant characteristics of the SOFCs is their ability for using hydrocarbons, apart from hydrogen, as fuel, by means of external or internal reforming. The cell itself generates the heat needed for fuel reforming. SOFCs are expected to play a crucial role in the transformation to a hydrogen economy, because they could take advantage of the current natural gas distribution network. SOFC's are particularly suitable for portable applications, because they can use almost any current commercially available liquid fuel. In fact, the commercialization of a small portable unit based in microtubular SOFC technology (2) to supply energy for mobile electronic devices is expected by the end of 2015 (3).

The core of the cell is the ionic conducting ceramic membrane, which acts as the electrolyte. Because of the unpaired mechanical and thermal stability, yttria stabilized zirconium oxide (YSZ) membranes are still the state of art electrolyte for SOFC. YSZ is a good oxygen ion conductor at temperatures above 800ºC (4). However there is a technical and practical interest in lowering the operation temperature of SOFCs. Lowering the operating temperature increases the long-term stability of the cell and permits the use of cheaper materials for the interconnectors and other stack components.

The most obvious way to lower the cell operating temperature is to reduce the electrolyte thickness. So, thin electrolytes are deposited using different techniques (dip-coating, spray-painting…) over one of the electrodes, usually the metal-ceramic porous composite Ni-YSZ anode (5), that operate as structural support of the cell. Anode supported configuration is probably the most prevalent Intermediate Temperature SOFC (IT-SOFC) configuration. The typical electrolyte thickness in this configuration is about 10-30 μm and the operation temperature around 700-800ºC (1). Nevertheless, cells with 100 nm thick YSZ electrolytes (the so-called micro-SOFC's) have been reported to be operative at lower temperatures with an output power density of 400 mW/cm^2 at 400ºC (6). Those devices are still far from commercialization due to thermal stability and mechanical stress issues. In addition, electrode-supported SOFC are also not free of problems. Apart from gas transport limitations because of the increased electrode thickness, which is necessary to act as structural support, its main problem is the redox stability of the structural support (7). An accidental failure of the fuel supply leads to re-oxidation of the metal particles in the anode, which undergo a volume expansion causing crack propagation. This mechanical damage leads to the degradation of the cell performance and, eventually, to its complete failure.

Alternatively to electrode-supported configurations, electrolyte-supported SOFCs are preferred in terms of mechanical robustness and resistance to redox cycles. In this configuration thin porous electrodes (30-50 μm) are deposited over a sintered electrolyte membrane. Thus gas transport inside the electrodes is not a problem and re-oxidation of the metal particles in the anode does not compromise the structural integrity of the cell. Another advantage is that the electrolyte can be sintered first at higher temperatures than the rest ceramic layers. As the electrolyte is the only dense and gastight ceramic layer of the cell, it usually requires the highest sintering temperatures. This minimizes reactivity problems between the different compounds during sintering and favors the achievement of the optimum porosity of the electrodes. However, the main inconvenience of this design is that electrolyte supported cells are prepared over 100–300 μm thick electrolytes and, as a consequence, they are designed to operate at high temperatures to reduce the ohmic resistance. The typical operation temperature of electrolyte supported SOFC is about 900-1000ºC for YSZ electrolytes. Higher temperatures are not usually used due to degradation problems (8).

A different approach, trying to combine the best of the electrode- and electrolyte-supported configurations, is to use laser machining to prepare thin self-supporting ionic conducting membranes. In precedent work we reported electrochemical results of laser machined single cells (9). We integrated the laser-machined membranes into single cells and showed that their performances met the expectations. By reducing the thickness of the electrolyte from 150 μm to 50 μm we decreased the Area Specific Resistance (ASR) of the electrolyte by a factor of 3. Laser engraving is being used in the last few years as a very suitable technique for achieving cost-efficient production of high quality ceramic parts. It allows obtaining excellent shaping, versatility, and accuracy, as well as highly controlled surface finishing if compared with conventional abrasive techniques for ceramic machining (10). With this method, the ceramic membranes are obtained from a thick and sintered ceramic plate by laser machining, although the same technique could be also applied to green-state ceramics (11). We use a pulsed laser in the nanosecond regime focused on the surface of the ceramic membrane. The beam spot is controlled by a couple of galvanometric mirrors. Consequently, we can efficiently reduce selected part of

the ceramic electrolyte, shaping the piece with a lateral resolution of about 10 μm and an in-depth resolution of about 3 μm. The membranes prepared with this method consist of a thin central region, ~20 μm in thickness and 8 mm in diameter, which is the electrochemically active area, surrounded by a ring ~150 μm thick, which is the mechanical support of the membrane where cell sealing can be performed. In addition to removal of material, pulsed laser produces plasma a plume of evaporated material that is deposited back into the mechanized surface in the form of electrolyte nanoparticles. The procedure can be scaled up to larger samples, simply by adding more adjoining thin areas separated by thicker zones, which act as support bars. The membranes have complete thermo-mechanical integration because both thin areas and supporting zones come from the same original sintered plate. Thus, they do not show problems of cracking due to thermal cycling. This is a major advantage compared to other types of preparation methods based in the deposition of thin membranes in holed supports because in that case the coefficients of thermal expansion of the membrane and the support are different (12).

In this paper we describe the laser-machining procedure for obtaining thin and self-supporting YSZ electrolyte membranes. The thickness and surface quality has been characterised by confocal optical profilometry and Scanning Electron Microscopy (SEM). Electron Back-Scattering Diffraction technique (EBSD) has been used to determine the in-depth profile of the residual stresses produced by the laser machining. Transmission Electron Microscopy (TEM), combining electron diffraction and Energy Dispersive Spectroscopy (EDS), has been used to characterise melted particle ejection during the ablation process, as well as the mechanisms of resolidification and redeposition on the surface. Finally, Electrochemical Impedance Spectroscopy (EIS) has been applied to test the electrical performance of the machined membranes.

Experimental Details

The starting ceramic samples were commercial 8YSZ (ZrO_2 doped with 8 mol% Y_2O_3) 50x50 mm^2 plates from Kerafol GmbH (Stegenthumbach 4–6, D-92676 Eschenbach, Germany). The original thickness of the plates was 150±15 μm. According to the manufacturer's specifications the ionic conductivity of the plates was σ>10 S/m at 850 ºC. Laser machining was performed using a Q-switched diode-pumped laser (model PowerLine S3 SHG, Rofin, Gunding, Germany) emitting at 532 nm. The laser's nominal power is 2 W, with a beam type TEM_{00} type, a quality factor M^2<1.2 and a repetition rate range of 15-400 kHz. The laser source was designed to ensure high beam quality, large depth of focus, and both pulse-to-pulse and long-term stability. All these characteristics are required in our application. The laser was equipped with a computer-controlled system of galvanometric mirrors to deflect the beam and scan the surface of the sample. Dedicated Computer Assisted Design (CAD) software defined the pattern machined over the sample (13). The focal distance of the lens was 100 mm, with 3.4 μm of the laser spot and a machinable area of 60x60 mm. The parallelism between the laser optics and the surface of the sample was ensured using optical grade mechanical components.

The depth and lateral dimensions of the machined areas were determined by optical profilometry using a confocal optical microscope (Model Sensofar PLμ2300, Nikon Instruments Europe B.V. Amstelveen, The Netherlands). The microstructural observations were performed using a scanning electron microscope (SEM); model Merlin

from Carl Zeiss NTS (Oberkochen, Germany). The specimens were Pt coated to avoid charging during the observations. The transmission electron microscope (TEM) experiments were performed in a 2000FXII microscope from Jeol (Tokyo, Japan). Both microscopes were equipped with an INCA-350 Energy Dispersive Spectroscopy (EDS) system from Oxford Instruments (Abingdon, Oxfordshire, United Kingdom). For the quantitative EDS experiments 8YSZ powder from Tosoh (TZ-8YSZ, Tosoh Corporation, Yamaguchi-ken, Japan) was used as standard (certified Y_2O_3 concentration: 13.82 wt%) to determine the Y-Zr sensitivity factor.

The EBSD experiments were carried out in the aforementioned SEM using a HKL detection system from Oxford Instruments. We used 500 μm thick YSZ plates of the same supplier and with the same characteristics as the 150 μm thick plates for investigating the extent of the mechanical damage underneath the processed surface. We machined grooves 130 μm in depth, 5x2 mm in wide, replicating the processing conditions used for preparing 20 μm thin membranes. The specimens for the EBSD experiments were prepared in cross-section embedded in epoxy resin and polished using a procedure previously applied to other ceramic samples (14). The samples were placed at 14.5 mm of working distance and tilted 70º towards the EBSD detector. The electron probe had 20 kV energy and 1.6 nA of current. To build-up the maps the electrons scanned the surface of the specimen and the ESBD patterns produced in every pixel was stored for subsequent off-line analysis. Patterns were recorded with 672x512 camera resolution (2x2 binning). To avoid charge up accumulation (YSZ is a non-conductive electronic material), charge was compensated in-situ using a dedicated gas injection system incorporated in the SEM (15). A fast first analysis was performed during acquisition to check the validity of the experiments. But the patterns were re-analyzed off-line using a slower but more accurate procedure. The parameters selected for the off-line analysis were level 4 for the AFI parameter, Hough resolution 100, 10 detected bands and 100 reflectors in the crystallographic phase (YSZ). Detailed description of all these parameters can be found in reference (16).

For the electrochemical tests, symmetrical cells of laser-machined and non-machined samples were fabricated by dip coating standard bilayer LSM/YSZ cathodes (17) on both surfaces. Pt paste was added to improve current collection. Samples were mounted on a commercial button-cell test rig (Probostat™ NorECs, Norway). Electrochemical measurements were performed using a Zahner Zennium (ZAHNER-Elektrik GmbH & Co.KG, Germany) workstation.

Experimental Results and Discussion

Laser Machining

The laser characteristics were chosen specifically for this application among commercially available and reliable laser sources working within the nanosecond ablation regime. Though YSZ is basically transparent in the visible region (9), it is possibly to drill YSZ ceramics using laser light with wavelength in the green region (532 nm) or even in the infra-red region (1064 nm) using solid-state lasers (18). High-intensity nanosecond pulses have been proved to be able to efficiently remove YSZ material by a photo-thermal laser ablation mechanism (19).

Several tests were carried out to determine the laser processing parameters. The optimum conditions were found using a repetition rate of 15 kHz and a scan speed of 150 mm/s. This resulted in a pulse separation of 10 μm along the scanning direction. The separation between the scanning lines was set the same as the one between the pulses. The optimum repetition rate is determined because in Q-switched lasers the pulse width varies as a function of the repetition rate, 15 kHz being the repetition rate at which the pulse width is the minimum in this laser (5 ns). In this case the pulse energy was 67 μJ. The position of maximum removal rate was experimentally determined (Figure 1). It was obtained placing the sample approximately 0.4 mm under the focus position. In this situation, the spot size is bigger, by a factor about 3 according to expression [1], where ω is the spot size, ω_0 is the spot size in the focus position, z the distance from the focus position and z_r the Rayleigh range (18). However, the area irradiated in every pulse still receives enough irradiance to evaporate the material (20). The removal rate averaged over all the scans needed to thin the samples was 0.01 mm^3/s.

$$\omega(z) = \omega_0 \sqrt{1 + \left(\frac{z}{z_r}\right)^2} \qquad [1]$$

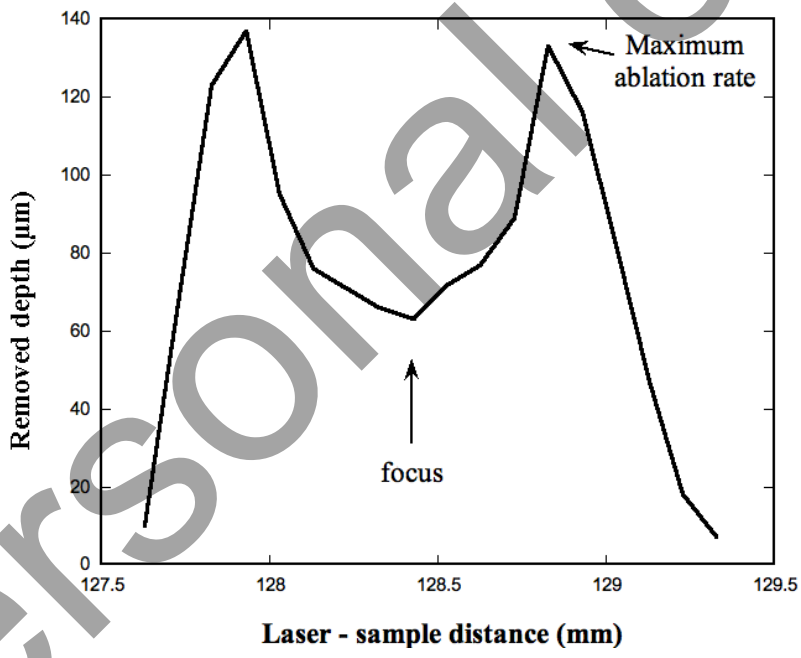

Figure 1. Removed depth as a function of the laser lens to sample distance. 20 scans at 15 kHz, v=150 mm/s and 10 μm line separation.

For the subsequent laboratory testing we prepared circular samples of 21 mm in diameter from squared commercial pieces of 50x50 mm and 150 μm thickness. The laser processed ~20 μm thin area was the central part of the ceramic piece of 8 mm in diameter and it was supported by an unprocessed ring with the original 150 μm thickness. After the laser thinning procedure, the circular piece was cut using the same laser machining system. An image of a machined sample can be observed in Figure 2a. Optical profilometry measurements indicated that parallelism between the surfaces of the machined area was preserved by a factor ~1/4000. A cross-section SEM image of a

fractured membrane is shown in Figure 2b. The only observed mechanical damage consists of small debonding between the grains close to the processed surface. The absence of cracks excludes any deterioration in the strength of the material at the engraved surface. The closed porosity observed already existed in the samples before the laser treatment.

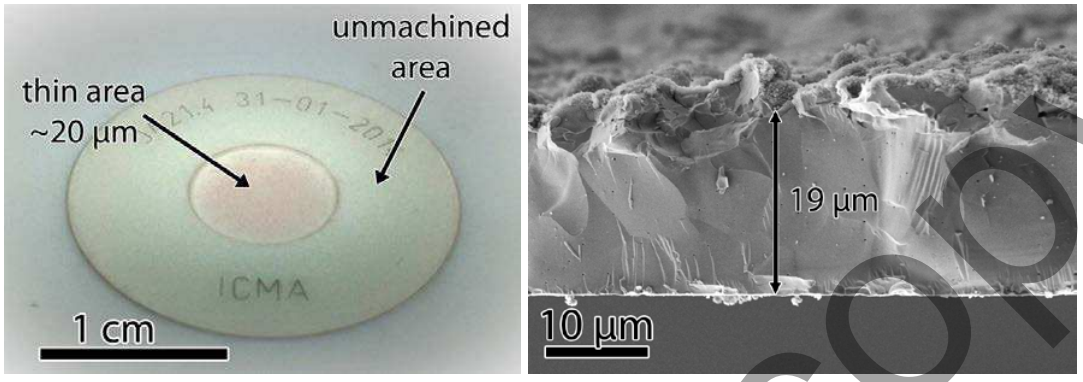

Figure 2. a) Image of a machined sample. b) SEM image of the fractured cross-section of a membrane.

Residual Stresses in the Membrane

During laser ablation in the nanosecond regime, part of the energy is thermally transferred to the sample. YSZ ceramic is a poor thermal conductor and the deposited laser energy will be contained in a relatively small region around the machined interface. Thus the ceramic surface gets heat very locally, suffering large temperature gradients that produce inhomogeneous thermal expansion. Thermal gradients may produce crack formation and, sometimes, even lead to the breakdown of the ceramic piece. In fact, the laser processing parameters are adjusted to prevent this. To get some insight about the depth of the heat-affected zone (HAZ) it is necessary to foreseen the mechanical performances of the membranes. EBSD has been used in the last few years to map the presence of both elastic and plastic strains in materials, this being a working theme in continuous progress (21). The residual stresses in a body can be categorized by the scale over which they are self-equilibrated (22). EBSD is very well suited to study type II (inter-granular) stresses, while type I (macro-stresses) or type III (atomic scale stresses) are better analyzed by X-ray and TEM techniques respectively. There are two main approaches for analyzing plastic strain using EBSD. The first one is based in the loss of pattern contrast due to the blurring of the Kikuchi bands edges by the presence of strain, mainly plastic, in the diffraction volume (23). However, pattern sharpness is affected by many other factors, the orientation of the crystal lattice being one of them. Thus, this is not an appropriate method for polycrystalline materials. We used the approach based in the local variations of lattice orientations due to the presence of dislocations (24). In this way we used the *Strain Contouring Component* of the proprietary software of the EBSD equipment (16). It measures the maximum misorientation between any two points in a grain and then weights this grain according to the misorientation value.

Large maps covering areas 200 μm underneath the machined surface were obtained. However, as the microstructural affectation was limited only to the superficial layer of the membrane, the results shown in Figure 3 are limited to this zone. Figure 3a is an

EBSD orientation map in which a different color is assigned to every crystallographic orientation. The grains are identified because they are formed by a set of connected pixels with the same crystallographic orientation, i.e. same color. The mean grain size was 1.9 μm and the standard deviation 1.1 μm. In addition to the orientation map, grain boundaries were marked in Figure 3a using black lines. The criterion was that the misorientation between adjacent pixels was higher than 1°. In Figure 3a, apart from an inner grain in which the boundaries are due to the presence of twins, only the superficial grains showed assessable local misorientation, evidenced by presence of sub-grain boundaries. In Figure 3b the *Strain Contouring* is directly represented, the half-width for smoothing being 1 μm. The color scale, varying from blue (low misorientation) to red (high misorientation), and the contour lines evidence the local misorientation originated by the plastic strain. This plastic strain affects, within the experimental limits of our experiments, to a layer of about 5 μm in depth. Thus, it only involves, at maximum, one or two of the most superficial YSZ grains. This finding is consistent with that could be expected. In laser ablation with nanosecond pulses, the heat-affected zone out of the ablated volume is related to melting. In the simplest approximation, the width of the HAZ can be estimated from the heat penetration depth $l_T \sim 2(D\tau_l)^{1/2}$, where D is the thermal diffusivity and τ_l the pulse width (18). Typical values for l_T in YSZ are about 0.1 μm.

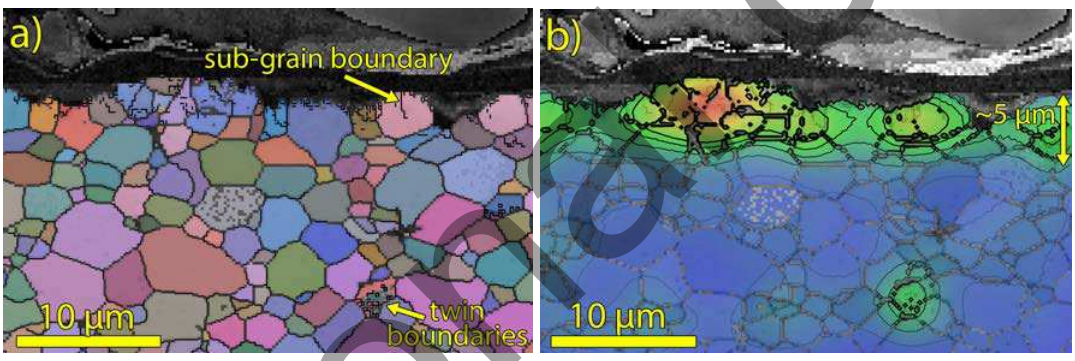

Figure 3. a) EBSD crystallographic orientation map of the superficial area of a laser-machined YSZ membrane. Grain boundaries higher than 1° are marked by black lines. b) EBSD map of the same area representing the *Strain Contouring* component.

A small word of caution about the interpretation of these results. Despite charge compensation, the edge of non-conductive ceramic samples is the most sensitive zone to charging in the SEM. This may produce some blurring of the EBSD patterns that could produce part of the measured local misorientation. Thus, the same experiments were performed at the edge of non laser-processed plates. In this case the area showing local misorientation is about 1 μm depth. As a consequence, we can conclude that the strained zone of the laser-processed membrane would be less than 5 μm deep.

Membrane Surface

The surface roughness of the processed membrane surface determined by optical profilometry was R_a=2.5 μm,. It is affected by the processing parameters, such as pulse separation and overlapping. These parameters were selected to minimize the surface roughness caused by laser processing. Photothermal ablation is the main mechanism involved in this process. Pulse width of 5 ns that yields to irradiance values above 11

MW/cm^2 is enough to produce high temperature gradients and local heating along the grain boundaries. Consequently, melting and vaporization start due to laser absorption by scattering mechanisms occurring at grain boundaries. Energy absorption, combined with the mechanical shockwave generated by the plasma plume produces intergranular breaking and subsequent ejection of material from the surface (10). This is consistent with the observation of small cracks at the grain boundaries of the superficial grains and the matching between the surface roughness and the grain size.

In addition, a thin layer of nanoparticles coats the processed surface, as shown in the Figure 4. The nanoparticles are formed either by molten liquid ejection during the ablation process, followed by the subsequent resolidification and deposition onto the surface, or also by direct ejection of particles directly ablated from the surface by intergranular breaking and thermal shock mechanisms that may show sharpen edges and much bigger sizes. This is consistent with previous results in other highly dense heterogeneous ceramics showing a bimodal and wide particle size distribution similar to the one observed in this case (25). As a consequence, laser machining not only reduced the membrane thickness, but also modifies the electrolyte surface. This could affect the electrolyte-electrode contact, and thus the electrode polarization as it will be discussed later.

Therefore, we have characterized the nanoparticles deposited on the membrane surface during the ablation process. They were collected placing TEM grids in the unprocessed zones during laser machining. Apart from the biggest particles, which were no collected in the TEM grids, two different types of nanoparticles were observed: spherical ones, with diameters between 200-500 nm, and clusters of very small nanometric particles, 3-4 nm in size. TEM images of both types of particles are included in Figure 5. Electron diffraction experiments confirmed, in both, cases that the crystal phase of the nanoparticles was the same as the original YSZ phase (26). Quantitative elemental analysis was done by EDS using the Cliff-Lorimer method and thin film approximation (27). The Y-Zr sensitivity factor was experimentally determined using 8YSZ powder. The results were 7.8±0.4 Y_2O_3 mol% for the spherical particles and 8.4±1.9 for the clusters of smaller nanoparticles. In both cases, Y content was compatible with the 8YSZ composition.

Therefore, the "solidified from melt debris" of the ablation process deposited over the membrane surface is formed by nanoparticles of the same nature that the electrolyte, 8YSZ. The macroscopic roughness of the membrane surface approximately corresponds to the grains size of the starting ceramic plates. This surface modification could affect for the electrochemical contact with the electrodes. In fact, Electrochemical Impedance Spectroscopy (EIS) studies of symmetrical cells (LSM/YSZ-YSZ-LSM/YSZ) showed a small decrease in terms of polarization resistance for the machined sample, in comparison with a standard and smooth surface sample (between 3 and 7.5% decrease depending on the temperature), as shown in Table I. This decrease of the ASR value could be attributed to a better adherence between the electrolyte and the electrode as a consequence of the presence of redeposited nanoparticles during laser processing.

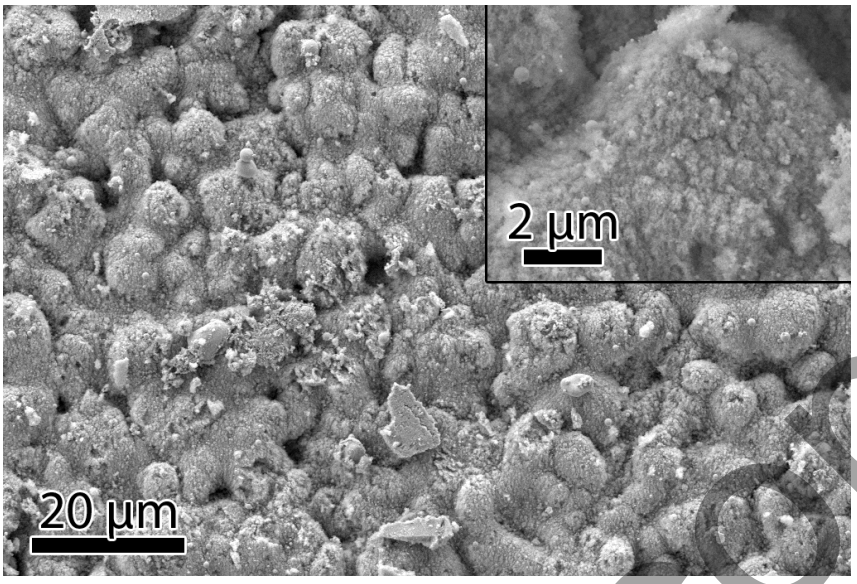

Figure 4. SEM images of the surface of the processed membranes. Top-right inset shows a higher magnification detail.

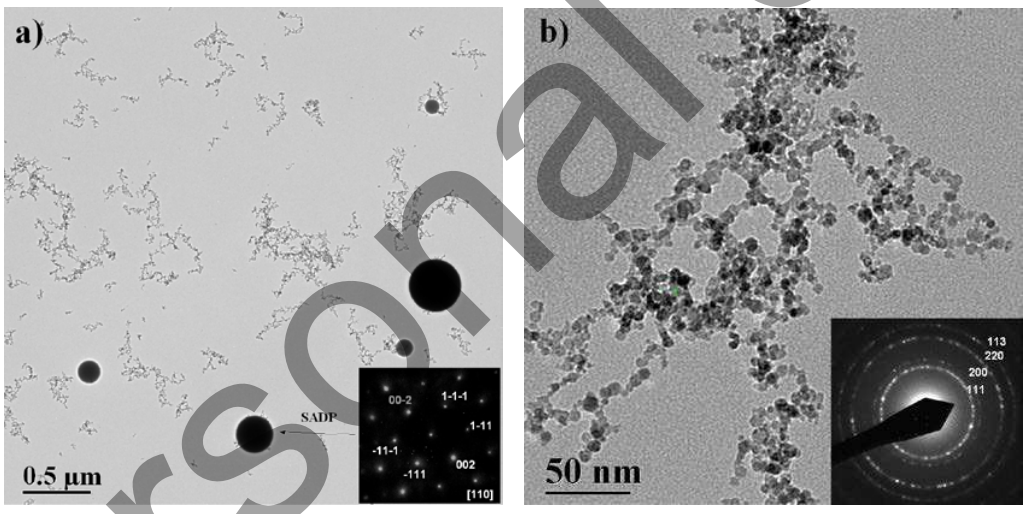

Figure 5. TEM images of particles ejected from the ceramic surface during the ablation process. a) General view showing the two types of resolidified particles. The inset is the selected area diffraction pattern (SADP) of the spherical particle along the [110] zone axis. b) Image of a cluster of the smaller nanoparticles. The inset shows the diffraction rings obtained in mode SADP, indexed according to the YSZ fluorite structure.

TABLE I. Polarization resistances of laser-machined and un-machined membranes ($\Omega \cdot cm^2$).

Temperature (ºC)	Un-machined samples	Machined samples	Polarization decreasing (%)
650	4.03	3.85	4.60
700	1.94	1.80	7.57
750	0.98	0.92	6.49
800	0.53	0.50	4.61
850	0.29	0.28	3.05

Conclusions

Pulsed laser ablation in the nanosecond regime has been proved as a useful tool for preparing thin and self-supporting ceramic electrolytes. We were able to prepare membranes with a 20 μm thick electrochemical active area with a diameter of 8 mm. An unprocessed 150 μm thick zone supports this area. The self-supporting membranes do not show problems of cracking due to laser processing Moreover, as both thin and thick zones come from the same sintered YSZ plate they have complete thermo-mechanical integration. Electron Backscattering Diffraction (EBSD) has been used to study the in-depth distribution of plastic strains. This constitutes a signature of the presence of residual stresses produced by non-uniform local heating during the laser machining. The heat-affected layer is less than 5 μm in depth. The machined surface has been studied by scanning and transmission electron microscopy (SEM and TEM). A thin layer of 8YSZ nanoparticles coats the processed surface. We have checked that this layer is not detrimental for the electrochemical performance of the membranes. On the contrary, Electrochemical Impedance Spectroscopy (EIS) experiments showed that the polarization resistance of LSM/YSZ cathodes deposited on the membranes decreases by about 5% in the 650-850 ºC temperature range, in comparison with unmachined YSZ plates.

Acknowledgments

This study was funded by the MAT2012-30763 project, which is financed by the Spanish Government (Ministerio de Economía y Competitividad) and the Feder program of the European Union. Authors would like to acknowledge the use of *Servicio General de Apoyo a la Investigación-SAI, Universidad de Zaragoza*. We are also grateful to M. Rötzer and D. Seitz at Rofin-Sinar Laser GMBH (Günding, Germany), for their advice and access to their facilities.

References

1. S.C. Singhal and K. Kendall, *High Temperature SOFCs: Fundamentals, Design and Applications,* Elsevier, Oxford (2003).
2. V. M. Orera, M. A. Laguna-Bercero and A. Larrea, *Frontiers in Energy Research* **2:**22 (2014).
3. http://www.ezelleron.eu/en/.
4. N. Q. Minh, *J. Amer. Ceram. Soc.* **76**, 563-588 (1992).
5. W. Z. Zhu and S. C. Deevi, *Mat. Sci. Eng. A* **362**, 228-239 (2003).
6. H. Huang, M. Nakamura, P. Su, R. Fasching, Y. Saito and F. Prinz, *J. Electrochem. Soc.* **154**, B20-B24 (2007).
7. D. Sarantaridis and A. Atkinson, *Fuel Cells* **7**, 246-258 (2007).
8. C. C. Appel, N. Bonanos, A. Horsewell and S. Linderoth, *J. Mater. Sci.,* **36**, 4493-4501 (2001).
9. A. Larrea, D. Sola, M. A. Laguna-Bercero, J. I. Peña, R. I. Merino and V. M. Orera, *J. Electrochem. Soc.*, **158**, B1193-B1197 (2011).
10. R. Lahoz, G. F. de la Fuente, J. M. Pedra, and J. B. Carda, *Int. J. App. Ceramic Tech.,* **8,** 1208-17 (2011).

11. J. Gurauskis, D. Sola, J. I. Peña, V. M.- Orera, *J. Eur. Ceram. Soc.*, **28,** 2673-2680 (2008).
12. C. D. Baertsch, K. F. Jensen, J. L. Hertz, H. L. Tuller, S. T. Vengallatore, S. M. Spearing and M. A. Schmidt, *J. Mater Research* **19**, 2604-15 (2004).
13. VisualLaserMarker User's Manual Version 5.0, ROFIN-SINAR Laser GmbH.
14. S. Serrano-Zabaleta, M. A. Laguna-Bercero, L. Ortega-San-Martin and A. Larrea, *J. Eur Ceram Soc* **34,** 2123-32 (2014).
15. S. Serrano-Zabaleta, H. Stegmann, C. Waltenberg and A. Larrea, *Microsc & Anal,* September **8,** 23-27 (2013).
16. Channel 5. Oxford Instruments HKL®. *HKL Technology 2006*. Denmark.
17. H. Monzón, M.A. Laguna-Bercero, A. Larrea, B.I. Arias, A. Varez, B. Levenfeld, *Int. J. Hydrogen Energy* **39**, 5470-5476 (2014).
18. D. Sola and J. I. Peña, *Materials,* **6**, 5302-13, (2013).
19. D. Bäuerle, "Laser Processing and Chemistry," 4th ed. Springer-Verlag Berlin Heidelberg, (2011).
20. D. Sola, A. Escartin, R. Cases and J. I. Pena, *Appl. Surface Sci.* **257,** 5413-19 (2011).
21. S. I. Wright, M. M. Nowell and D. P. Field, *Microsc. Microanal.* **17,** 316-29 (2011).
22. P. J. Withers and H. Bhadeshia, *Mater Sci & Technology*, **17**, 355-65 (2001).
23. N. C. K.Lassen, D. J. Jensen and K. Conradsen, *Mater Sci Forum* **157-162**, 149-158 (1994).
24. D. P. Field, *Mater Sci & Eng A,* **190**, 241-246 (1995).
25. R. Lahoz, J.M. Pedra, J.B. Carda and G.F. de la Fuente. Presented at the 3rd International Congress on Ceramics, (2010), Ceramic Society of Japan, Osaka, Japan.
26. D. G. Lamas and N. E. Walsoe de Reca, *J. Mat. Sci.*, **35**, 5563-5567 (2000).
27. G. Cliff and G. W. Lorimer, *J. Microscopy-Oxford,* **103**, 203-07 (1975).